Science Advances
AAAS

advances.sciencemag.org/cgi/content/full/4/10/eaat9700/DC1

Supplementary Materials for

Gravitational collapse of Mount Etna's southeastern flank

Morelia Urlaub*, Florian Petersen, Felix Gross, Alessandro Bonforte, Giuseppe Puglisi, Francesco Guglielmino, Sebastian Krastel, Dietrich Lange, Heidrun Kopp

*Corresponding author. Email: murlaub@geomar.de

Published 10 October 2018, *Sci. Adv.* **4**, eaat9700 (2018)
DOI: 10.1126/sciadv.aat9700

This PDF file includes:

Supplementary Text
Fig. S1. Close-up bathymetric map and seismic image of the area with the seafloor geodetic network.
Fig. S2. Relative changes in distances for all 10 baselines during the entire observation period from April 2016 to July 2017.
Fig. S3. Cosine relationship between the relative distance shortening and lengthening during the May 2017 event and the angle at which the baselines cut the fault trace.
Fig. S4. Relative pressure differences for the entire observation period (10-day moving average) between individual transponder pairs.
Fig. S5. GPS displacements referring to the April 2016 to July 2017 comparison.
Fig. S6. Ascending 31 March 2016 to 30 July 2017 and descending 6 April 2016 to 30 July 2017 Sentinel-1 phase interferograms.
Fig. S7. East, north, and up displacement components resulting from the SISTEM integration.
Fig. S8. Ground displacements along the LOS across the study area measured by both Sentinel 1A and 1B satellites with a 6-day interval.
Reference (*40*)

Supplementary Materials

Supplementary Text

Seismic and bathymetric characteristics of the offshore boundaries of Mount Etna's unstable flank

The northern boundary of the onshore unstable sector is the seismically active left-lateral Pernicana Fault, which splits up into several smaller scale fault systems near the coast (*17, 26)*. The latter fault systems are aseismic and deformation appears diffuse. This is similar offshore, where no clear structure is evident, but Riposto Ridge forms a morphological boundary (*24*). In the south, the right-lateral Tremestieri-Trecastagni fault zone, which appears to merge near the coastline to the Acitrezza fault (*26*), transfers extension to the East (*17*). The fault outcrop extends beyond the coast (*13*) and on to a morphologically prominent structural feature north of Catania Canyon (e.g. Fig. 1), termed 'lineament' (*13, 24*).

Regional seismic reflection lines reveal that the lineament coincides with discontinuous strata in the shallow subsurface indicating active tectonic deformation (*24*). The deformation pattern has been interpreted as a positive flower structure indicative of a right-lateral oblique transpressive fault system (*24*). New closely spaced high resolution seismic profiles across the lineament, which were collected in 2016 during RV POSEIDON expedition POS496 support this interpretation. Fig. S1 shows a seismic line from the POS496 survey, which crosses the lineament in the area of the seafloor geodetic array. At kilometer 3.3, i.e. the location of the lineament, seismic reflectors are sharply truncated. Whereas reflectors to the south appear predominantly horizontally layered, reflectors to the north are slightly tilted northwards. The structural discontinuity and the truncation of seismic reflectors lend support to the interpretation that the lineament is the surface expression of an active underlying strike slip fault. The data recorded by the geodetic array that measures across this strike slip fault confirm this observation and we therefore interpret the lineament north of Catania Canyon as the southern boundary of the unstable flank.

Results of seafloor displacement monitoring campaign

Data download in July 2017 during RV Poseidon expedition POS515 provides continuous time series for an observation period of almost 16 months without interrupting the long-term monitoring campaign. The stations were recording all parameters (travel times, sound speed, pressure, temperature, tilt) with the exception of transponder 2 that shows a data gap in June-July 2016. Transponder 1 recorded data correctly but data download was corrupt. However, both transponders were continuously answering to incoming acoustic signals resulting in one-directional baselines.

Distance changes

Changes in the acoustic measurements of distances may result from a combination of true length variations and drift in the computed sound speeds used in the time-to-distance conversion. This makes it hard to differentiate very long period displacement signals from drift. However, it is with large certainty that the length changes recorded in May represent deformation on a strike-slip fault because it is observed in all of the six fault-crossing baselines (fig. S2). The changes in lengths clearly stand out of the background noise level and data scatter. Standard deviations range between 2 mm for the shortest baseline (transponder pair 2-5) and 20 mm for one of the longer baselines (pair 2-3) (fig. S3) and is smaller than the observed baseline change.

For some transponder pairs we note a change in distances to the opposite direction prior to the main May 2017 event as well as an overshoot to more extreme distance changes during the event

(e.g. 1-3, 2-4, 3-4, 4-5 in fig. S2). The same pattern also shows up in the pressure baselines (fig. S4). Such a signal has been observed during slow-slip events elsewhere (*43*). A possible explanation is that sliding of the southern side of the fault is triggered during the slow-slip event. This may well affect only the very shallow sediments, but we do not have any constraints on that. We therefore do not consider the overshoot, which is the common consensus (*43*).

The changes in distance between two transponders are the sum of horizontal and vertical movements of both transponders. Acoustic distances are not sensitive to height changes and therefore changes in acoustic distances reflect horizontal displacement. For example, for an original transponder pair distance of 1000 m with height difference of 100 m (approximate averages in the geodetic network), a relative change in depth of one transponder of 0.1 m is required to explain a distance change of 0.01 m.

Cosine relationship of displacement and fault angle
Relative distance changes during the May 2017 event range between 6 mm and -39 mm for different transponder pairs. These variations are in line with the network geometry and the strike direction of the fault relative to the baselines. The measured relative distance changes between transponder pairs are a function of the slip on the fault and the angle at which the baseline crosses the fault. A very small angle provides a minimum estimate of fault slip. Our data show that the fault trends between transponders 1 and 3. Owing to the network geometry, the baseline between these stations and the fault itself cross at very small angle, so that the change in acoustic distance between transponders 1-3 may be regarded as the best estimate of fault slip. Figure S3 shows that the acoustic distance changes recorded by other transponder pairs that cross the fault fit extremely well with the expected cosine relationship.

Estimated magnitude and characteristics of the May 2017 offshore event
The cumulative aseismic moment released in the May 2017 offshore event is Mw 4.3 - 5.37 assuming fault plane lengths ranging between 5 -15 km, fault depths between 0.5 and 5 km, and a shear modulus of 30 GPa (*27*). With its duration of eight days and an estimated moment magnitude between 4.3 and 5.3 the Mount Etna offshore event in May 2017 classifies as a slow slip event (*40*). The phenomena of slow earthquakes or ‘slow slip events’ (SSE) are mainly observed at convergent plate boundaries. Observations of SSE on strike-slip faults are extremely rare. Under water as yet only the vertical component has been detected by pressure gauges.

<u>Onshore data</u>
Data from the permanent GPS monitoring network of Etna acquired during the first week of April 2016 and the last week of July 2017 were processed for calculating the cumulative displacements (fig. S5). To investigate the deformation during the observation period, we also performed a Differential Interferometry Synthetic Aperture Radar (DInSAR) analysis of ascending and descending Sentinel 1A/1B TOPSAR images.

We analyzed the ascending 31 March 2016-30 July 2017 and the descending 06 April 2016–30 July 2017 pairs (fig. S6). The SISTEM results (fig. S7) depict the 3D ground deformation occurring during the April 2016-July2017 time span; they show an inflation affecting the summit central area of the volcano (with an uplift of about 5 cm), coupled with an eastward movement of the eastern flank (maximum value of about 7 cm recorded along the Pernicana fault). Another important feature of the 3D deformation pattern obtained by integrating GPS and InSAR data is the clear control of the main fault system (Pernicana fault, at the northern flank, and Acicastello fault, in the south) on horizontal displacements.

Supplementary Figures

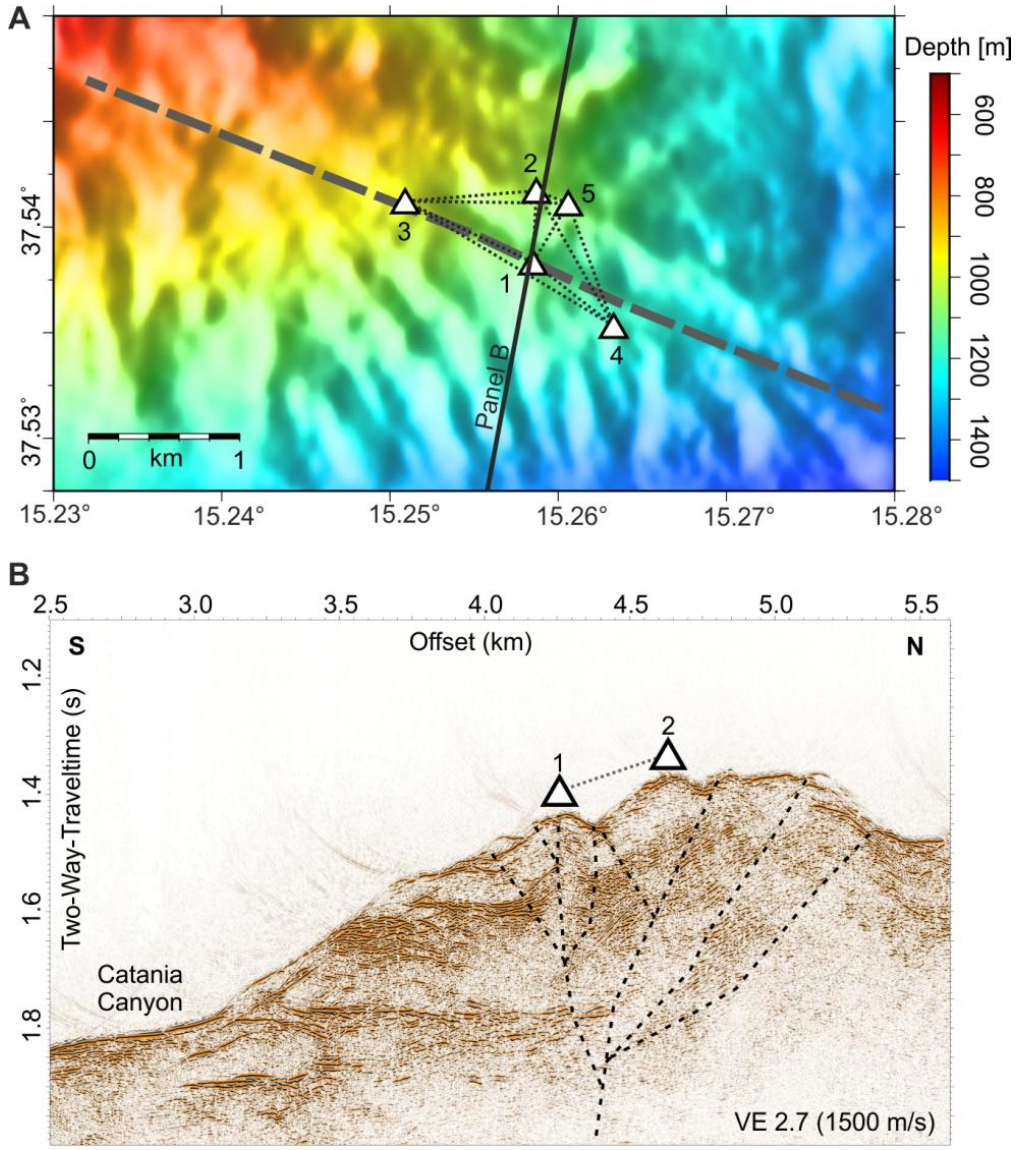

Fig. S1. Transponder locations shown on local bathymetry (A) and high resolution seismics (B). (A) Triangles represent transponders with individual numbers. (B) Part of seismic profile p500 crossing the seafloor geodetic array recorded with a Geometrics GeoEel streamer consisting of 11 solid state sections (each 12.5 m). One standard 2 * 0.2l Mini-GI-gun was used as source. Triangles above the seafloor indicate projected transponder locations.

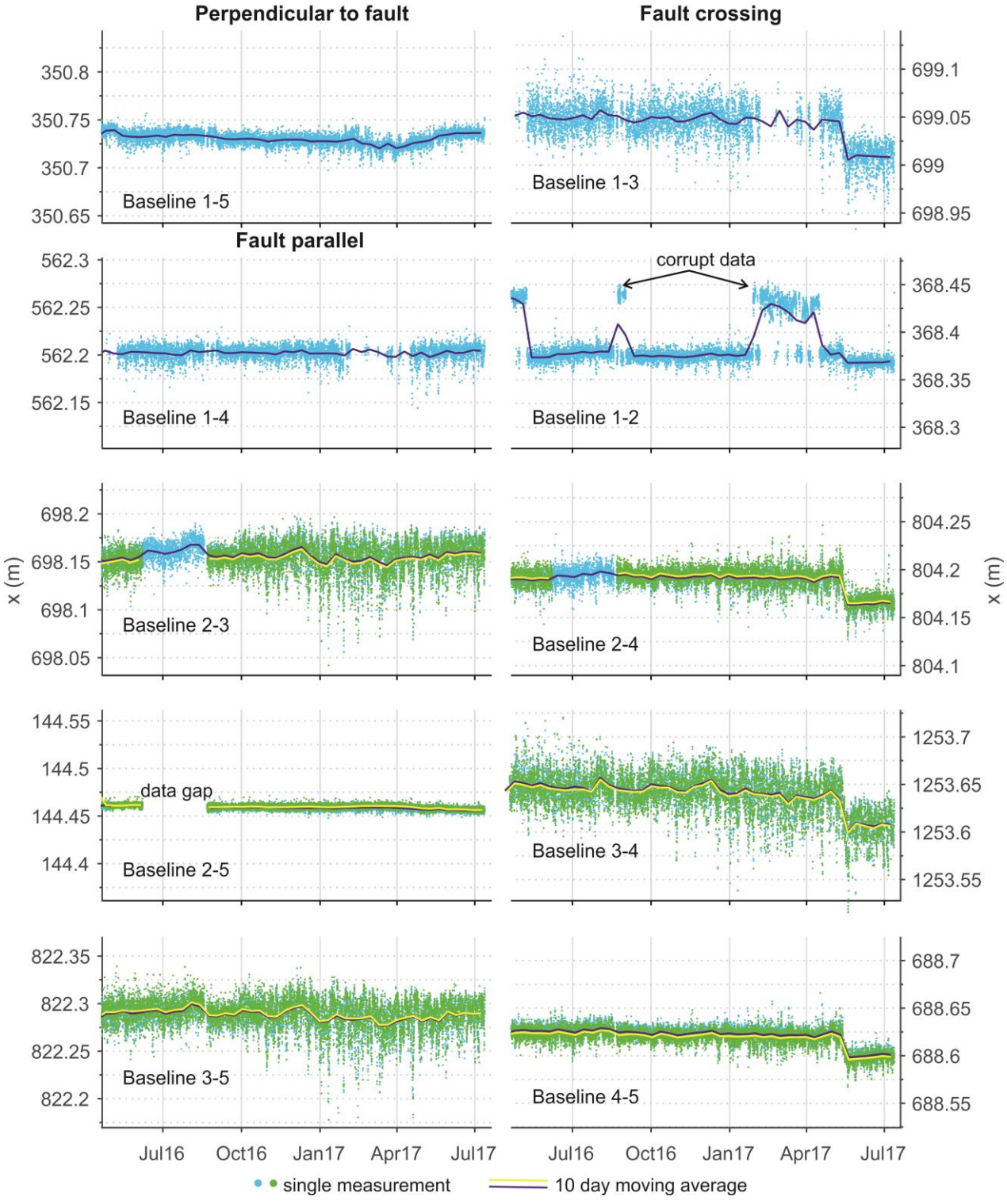

Fig. S2. Relative changes in distances for all 10 baselines during the entire observation period from April 2016 to July 2017. Blue and green markers indicate active interrogation and passive response of acoustic signals, respectively. Due to high sampling frequency individual measurements partly overlap. Dark blue and yellow lines show a 10 day moving average also for interrogation and response. Transponder 1 did not record any data but was still responding to the interrogations of all other transponders. All plots show a range of 0.2 m. For transponder locations see fig. S1A.

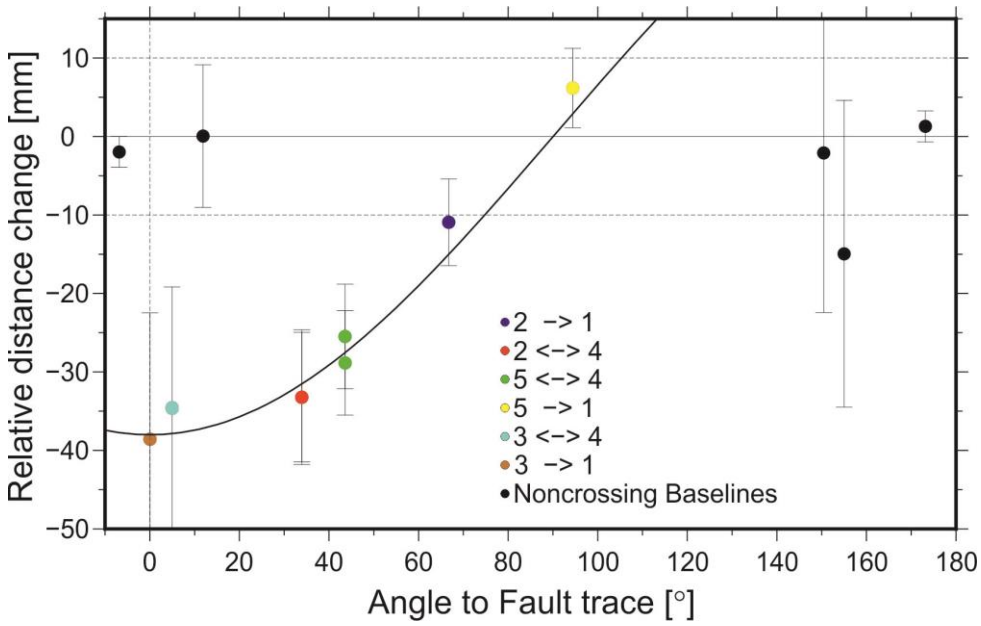

Fig. S3. Cosine relationship between the relative distance shortening and lengthening during the May 2017 event and the angle at which the baselines cut the fault trace. Error bars represent the standard deviation of the baseline time series before 10 May 2017. For transponder locations see fig. S1A.

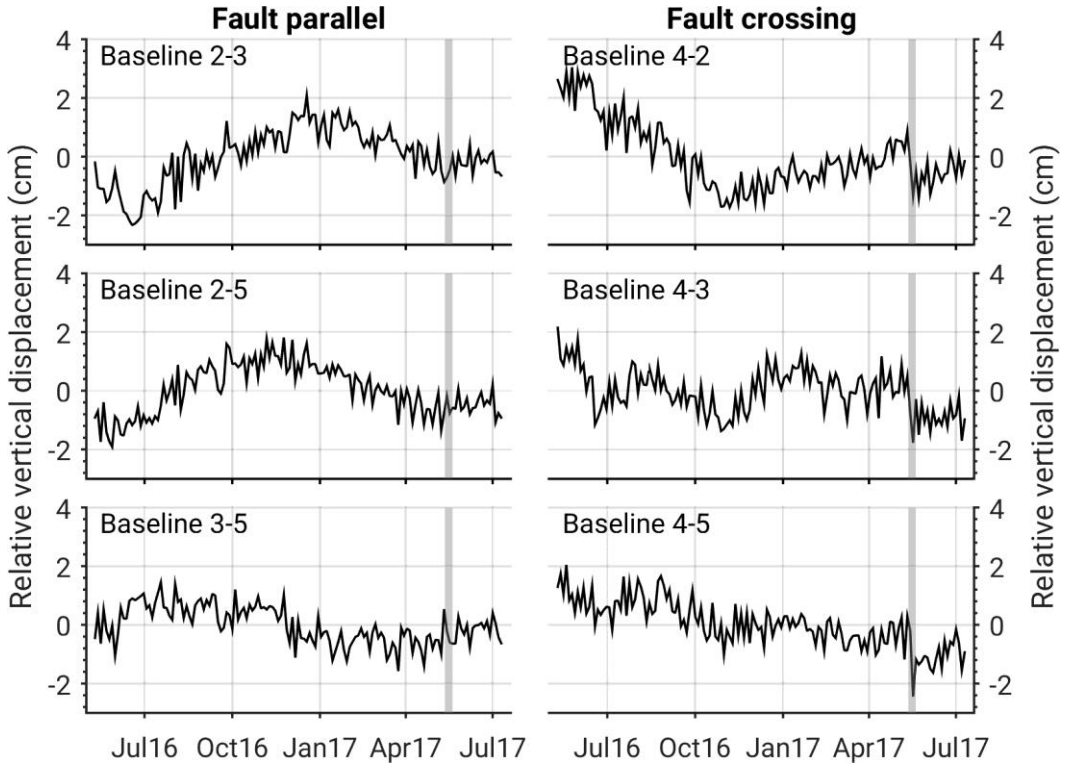

Fig. S4. Relative pressure differences for the entire observation period (10-day moving average) between individual transponder pairs. The displacement of the second transponder relative to the first is shown (e.g. in A the vertical displacement of transponder 3 relative to transponder 2 is shown, i.e. transponder 2 is assumed fixed). Left panels show transponder pairs north of the fault and right panels show transponder pairs crossing the fault. Grey vertical bars represent the time period of the May 2017 event. We do not show time series for baselines of transponder 1 because it recorded corrupt data. The May 2017 event is evident in all fault crossing transponder pairs in that all stations on the northern side of the fault move downward by approximately 10 mm with respect to transponder 4. Long period signals occur in all transponder pairs and do not reflect true vertical displacement but are the result of seasonal temperature variations. For transponder locations see fig. S1A.

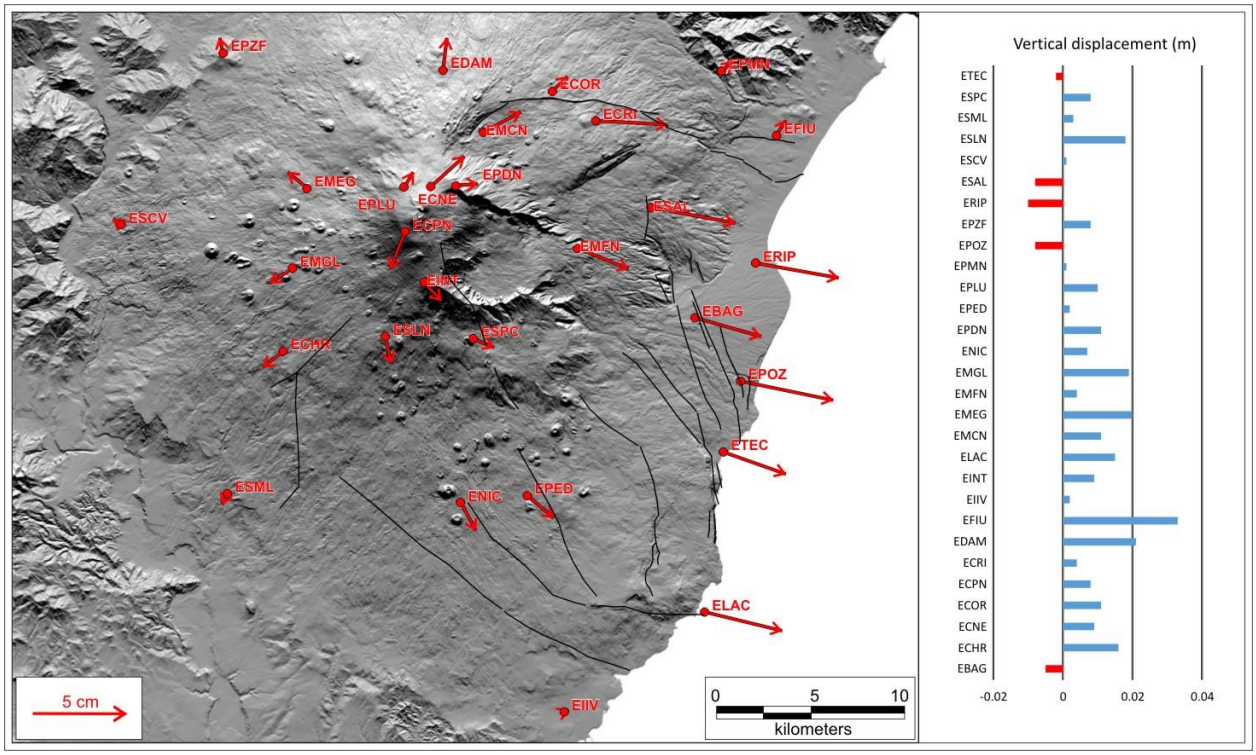

Fig. S5. GPS displacements referring to the April 2016 to July 2017 comparison. Red vectors in the map indicate the observed horizontal displacements. On the right, vertical displacement is reported for each station.

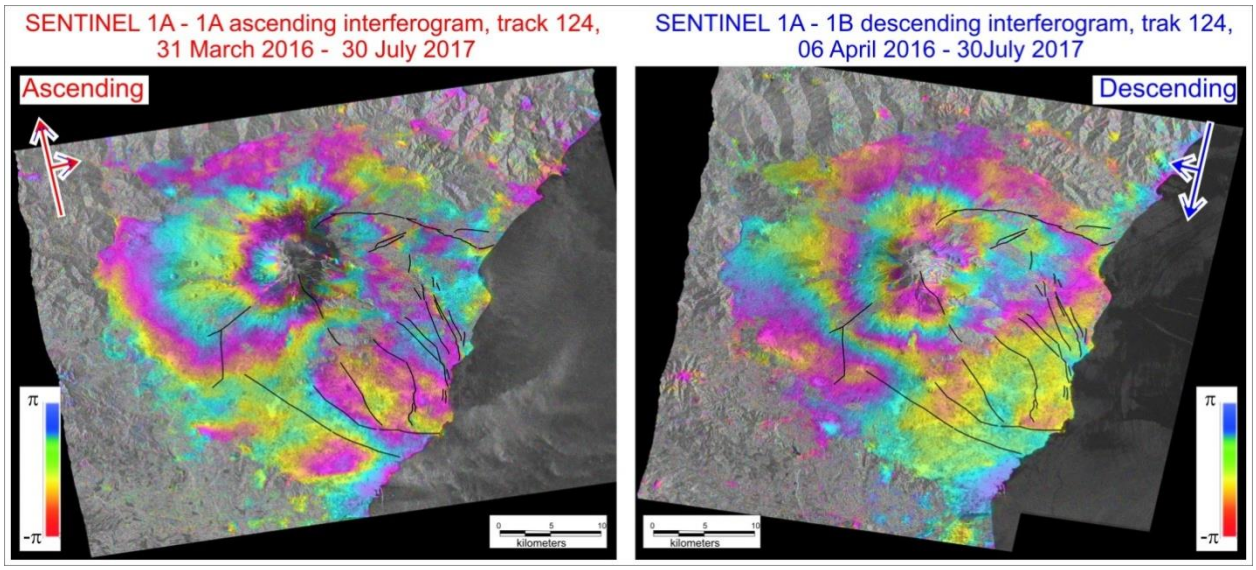

Fig. S6. Ascending 31 March 2016 to 30 July 2017 and descending 6 April 2016 to 30 July 2017 Sentinel-1 phase interferograms. Ascending 31 March 2016 to 30 July 2017 (left) and descending 06 April 2016 to 30 July 2017 (right) Sentinel-1 phase interferograms. Fault traces (*26*) are reported in the figure in order to demonstrate how the main discontinuities in the ground deformation field are controlled by the local fault systems.

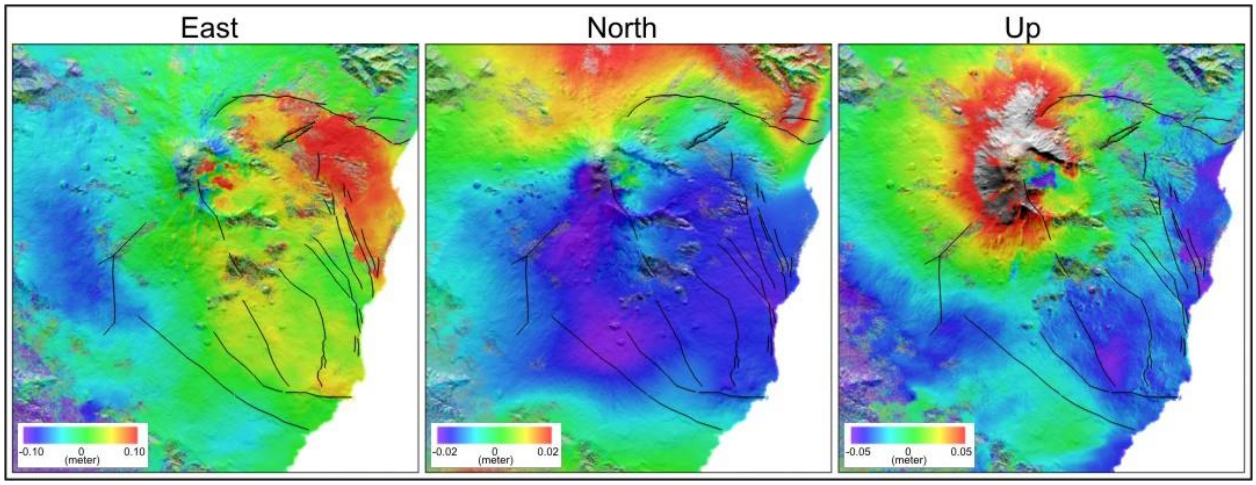

Fig. S7. East, north, and up displacement components resulting from the SISTEM integration. Fault traces (*26*) are reported in the figure in order to evidence how the main discontinuities in the ground deformation field are controlled by the local fault systems.

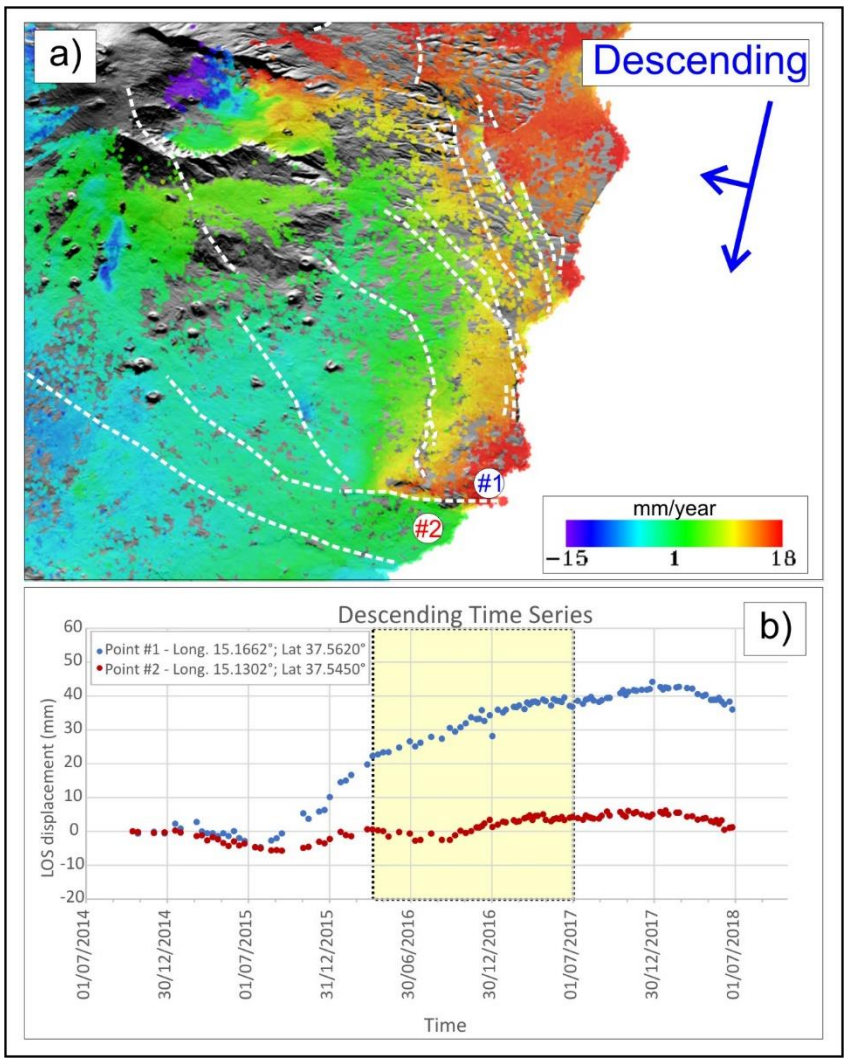

Fig. S8. Ground displacements along the LOS across the study area measured by both Sentinel 1A and 1B satellites with a 6-day interval. (a) Descending Sentinel 1A-B mean LOS velocity (2014-2018); positive values approaching to the sensor. (b) Time Series of two selected points located on to northern and southern side of Acitrezza fault, respectively. The yellow rectangle represents the time period investigated by the offshore array.